International Journal of GEOMATE, Jan., 2024 Vol.26, Issue 113, pp.82-89
ISSN: 2186-2982 (P), 2186-2990 (O), Japan, DOI: https://doi.org/10.21660/2024.113.g13288
Geotechnique, Construction Materials and Environment

DEVELOPMENT OF A BAGHOUSE FILTER CFD MODEL FOR EFFICIENT PARTICULATE REMOVAL IN AIR FILTRATION SYSTEMS

Angtida Punyaponchai[1,2], Jetsadaporn Priyadumkol[1], Kittipos Loksupapaiboon[1,2], Sommart Thongkom[3] and Chakrit Suvanjumrat[1,2]*

[1]Department of Mechanical Engineering, Faculty of Engineering, Mahidol University, Salaya, Nakhon Pathom 73170 Thailand;
[2]Laboratory of Computer Mechanics for Design (LCMD), Department of Mechanical Engineering, Faculty of Engineering, Mahidol University, Salaya, Nakhon Pathom 73170, Thailand;
[3]Division of Mechanical Engineering, Faculty of Engineering, Bangkokthonburi University, Bangkok 10170, Thailand

*Corresponding Author, Received: 19 July 2023, Revised: 12 Dec. 2023, Accepted: 15 Dec. 2023

ABSTRACT: Air pollution poses a serious challenge for our capital city, and one crucial line of defense is effective dust control. Employing computational fluid dynamics (CFD), we designed a dust collector aimed at efficiently tackling particles smaller than 10 micrometers, a critical factor in combating air pollution. OpenFOAM, an open-source CFD software, was instrumental in this design process. Notably, our dust collector is equipped with bag filters capable of filtering PM 2.5. The application of the k-ε turbulence model governed the flow through the baghouse in our CFD model, while the bag filter was treated as a porous medium following Darcy's law. To validate our approach, we conducted an airflow experiment through a bag filter installed in the baghouse, determining the coefficient of Darcy's equation and benchmarking against CFD results. Impressively, our baghouse model exhibited an average error of less than 6.46%. This CFD-guided modeling not only minimizes trial and error in design but also provides manufacturers with insights to optimize and innovate baghouses in the future.

Keywords: Bag filter, Baghouse, Computational fluid dynamics, Porous media

1. INTRODUCTION

The baghouse finds widespread application in collecting particulate emissions from diverse industrial plants, including those dealing with milk, wood, fly ash, and limestone powder. This technology represents a significant leap forward in dust collection [1-3]. Within the baghouse, numerous bag filters, often constructed from nonwoven filter fabrics, are strategically assembled. These fabrics possess a random fiber structure, typically in sheet form, designed to effectively capture particulate matter from a moving fluid by entrapping it within its intricate structure. The filtration performance of nonwoven filter fabrics is gauged through considerations of air permeability and pore size distribution [4]. Air permeability, measured in accordance with standards such as ASTM D737, DIN 53887, or the standardized test EN ISO 9237, quantifies the rate of airflow passing perpendicularly through a specified area under a designated air pressure differential between the material's two surfaces. Typically, air permeability stands as a vital technical parameter among the data that manufacturers are obligated to disclose to their customers.

The evolution of baghouses often revolves around filter bags, typically of the cylindrical type, aimed at purifying the air and establishing a clean environment. To streamline the installation space required for baghouse dust collector systems, pleated filter cartridges have been introduced. However, it's worth noting that pleated bag filters, despite their space-saving advantages, exhibit lower filtration cleaning efficiency compared to their cylindrical counterparts when subjected to the same filtration velocity [5]. In an effort to optimize pleated filter bag geometry, Kim and Lee [6] conducted experiments to measure the effective filtration area of pleated filter bags. Their findings revealed that a ratio of pleated height to width at 2.21 resulted in the maximum effective filtration area. A critical factor influencing baghouse performance is can velocity, which represents the airstream velocity in the passage area between installed bag filters. Recognizing its significance, Joe et al. [7] delved into the study of velocity effects on a pilot-scale bag filter dust collector. Their recommendation included selecting an appropriate can velocity for real-scale equipment based on testing with the pilot-scale bag filter dust collector.

Developing a baghouse through experimental methods can be both cumbersome and expensive, leading researchers to opt for computational

approaches. In the study by Pereira et al. [8], the inlet positions of a baghouse equipped with 49 bags were investigated using computational fluid dynamics (CFD). They utilized streamlines and mass flow profiles within the baghouse to estimate filtering performance. Another computational study by Park et al. [9] focused on modeling a baghouse with a bag filter to analyze airflow patterns. Darcy's law-based porous media model was employed to simulate the bag filter within the baghouse. Their findings highlighted that the air filtration velocity became non-uniform when the filter bag exceeded a length of 3 meters, with the bottom section exhibiting a smaller filtration velocity compared to the top. In a different approach, Lin et al. [10] utilized CFD software to enhance the collection efficiency of elliptical filter cartridges with venturi. They justified the performance of these filter cartridges by analyzing the pressure drop resulting from airflow through the elliptical filter cartridge. Their research indicated that a venturi with a throat diameter of 160 mm exhibited superior cleaning effects for the elliptical filter cartridge.

2. RESEARCH SIGNIFICANCE

As mentioned earlier, Computational Fluid Dynamics (CFD) stands out as an advanced tool for the improvement and development of baghouses. The modeling of various types of bag filters has been explored to investigate baghouse performance, typically accomplished using commercial software. However, the high cost of such software poses a challenge, particularly for small and medium-sized industries. In response to this obstacle, the focus of this research is on developing a baghouse model utilizing open-source CFD software, specifically OpenFOAM. The methodology outlines the implementation of porous media on the bag filter model in a detailed manner. To benchmark the CFD model, a full-scale baghouse was fabricated and tested. Additionally, the accuracy of the CFD model was validated against experimental data, ensuring its reliability. This approach allows for the investigation of airflow through the bag filter. Ultimately, the developed baghouse model serves as a satisfactory and cost-effective guide for future baghouse development using open-source CFD software, eliminating the need for expensive licensing in subsequent endeavors.

3. GOVERNING EQUATIONS

3.1 Reynolds Averaged Navier–Stokes Model

The turbulent flow inside the baghouse filter is governed by the Reynolds-averaged Navier–Stokes (RANS) equations, which consist of continuity and momentum equations [11, 12]. In Cartesian coordinates, these equations can be expressed as follows:

$$\frac{\partial \bar{u}_i}{\partial x_i} = 0 \tag{1}$$

$$\frac{\partial \bar{u}_i}{\partial t} + \frac{\partial (\overline{u_i u_j})}{\partial \ x_j} = -\frac{1}{\rho}\frac{\partial \bar{p}}{\partial x_i} + \nu \frac{\partial^2 (\bar{u}_i)}{\partial x_i^2} + \frac{1}{\rho}\left[\frac{\partial\left(-\rho \overline{u_i' u_j'}\right)}{\partial x_i}\right] + \bar{S}_i \tag{2}$$

where $\bar{u}_i$, $\bar{p}$, ρ, ν, $\bar{S}$, $\rho\overline{u_i' u_j'}$, and u' denote the mean velocity component, mean pressure, fluid density, kinematic viscosity, source term, Reynolds stress term, and fluctuations in the velocity, respectively.

The randomness of fluid flow introduces a Reynolds stress term in the RANS equations. To approximate this Reynolds stress term, the concept of eddy viscosity was introduced by Boussinesq. The Boussinesq hypothesis relates the Reynolds stress to the velocity gradient and turbulent viscosity, and it is described as follows:

$$\rho\overline{u_i' u_j'} = -\frac{2}{3}\delta_{ij}k + \mu_t\left(\frac{\partial \bar{u}_i}{\partial x_j} + \frac{\partial \bar{u}_j}{\partial x_i}\right) \tag{3}$$

$$\mu_t = C_\mu \rho \frac{k^2}{\varepsilon} \tag{4}$$

Turbulence model

For simplicity, the Reynolds stress has a turbulence model as the variable. The two-transport equations turbulence model is the k-Ɛ turbulence model. The equations are

$$\frac{\partial(\rho k)}{\partial t} + \frac{\partial\left(\rho \bar{u}_j k\right)}{\partial x_j} = \frac{\partial}{\partial x_j}\left[\left(\mu + \frac{\mu_t}{\sigma_k}\right)\frac{\partial k}{\partial x_j}\right] - \rho\varepsilon + 2\mu_t S_{ij}\frac{\partial \bar{u}_i}{\partial x_j} \tag{5}$$

$$\frac{\partial(\rho \varepsilon)}{\partial t} + \frac{\partial\left(\rho \bar{u}_j \varepsilon\right)}{\partial x_j} = \frac{\partial}{\partial x_j}\left[\left(\mu + \frac{\mu_t}{\sigma_\varepsilon}\right)\frac{\partial \varepsilon}{\partial x_j}\right] + C_{\varepsilon 1} P_k \frac{\varepsilon}{k} - C_{\varepsilon 2}\rho\frac{\varepsilon^2}{k} \tag{6}$$

where μ_t, k, ε, and S denote the eddy viscosity, turbulent kinetic energy, turbulent kinetic energy dissipation rate, and strain rate tensor, respectively.

The constants for the k-ε model, denoted as C_μ, $C_{\varepsilon 1}$, $C_{\varepsilon 2}$, σ_k, and σ_ε, have specific values, where C_μ is 0.09, $C_{\varepsilon 1}$ is 1.44, $C_{\varepsilon 2}$ is 1.92, σ_k is 1.0, and σ_ε is 1.3 [13].

3.2 Porous media model

Darcy proposed a pipe friction formula that was later reduced to Poiseuille's linear equation. In the context of a filter bed, the rate of water flow through the bed is directly proportional to the area of the sand,

the difference in fluid head height at the inlet and outlet of the sand bed, and inversely proportional to the thickness of the bed [14]. The water flow through the filter bed in porous media can be expressed according to Darcy's law as follows:

$$\Delta p = -\frac{\mu L}{k}\bar{u}_i \tag{7}$$

where k denotes the permeability of porous media.

Friction arises from a combination of shear forces and pressure forces. Shear forces are described by a linear equation, whereas pressure forces are represented by a quadratic equation. The Darcy-Forchheimer equation establishes a relationship between the pressure loss due to friction across porous media and the velocity of the flow within the medium [15]. It is expressed as follows:

$$\Delta p = -\mu L D\bar{u}_i - \frac{\rho L}{2}F{\bar{u}_i}^2 \tag{8}$$

where D denotes a linear resistance coefficient and F denotes a quadratic resistance coefficient.

4. MATERIALS AND METHODS

Our study encompassed both experimental work and CFD modeling focused on the baghouse filter. Specifically, we designed and fabricated the baghouse filter to conduct experiments, testing the bag filters and using the results to benchmark the CFD outcomes. Simultaneously, a comprehensive baghouse filter model was developed to investigate the filter and flow characteristics within the baghouse system. This model has the potential to predict the pressure drop of the baghouse filter under various conditions, particularly when the bag filter is constructed using different nonwoven fabrics. This dual approach, combining experimentation and modeling, enhances our understanding of the baghouse filter's behavior and performance across diverse material configurations.

4.1 Bag Filter Testing

The baghouse design, depicted in Figure 1, facilitates the installation and replacement of a single filter cartridge through the top covered plate. The aerosol inlet is strategically positioned on the hopper's wall, which includes a dust outlet at its bottom for efficient collection and discharge of dust through the dust-discharging device. Centrally located within the squared housing, the bag filter is easily accessible for inspection through the designated inspection door. Post dust entrapment by the bag filter, purified air is released through the outlet at the top of the baghouse. A circular duct connects the air outlet to an electric blower

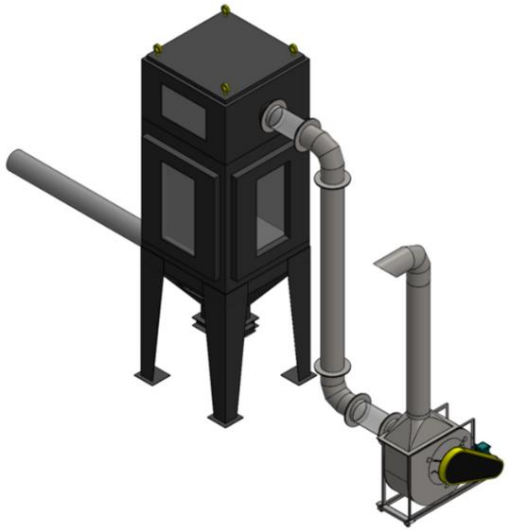

Fig. 1 The baghouse design

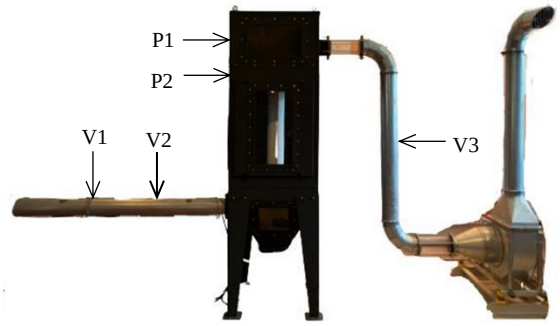

Fig. 2 Measurement points on the baghouse filter

responsible for drawing in and releasing the clean air into the environment. To regulate the filtration velocities of the baghouse, a blower inverter is utilized, allowing for frequency adjustment ranging from 10 to 50 Hz in this study.

The fabricated baghouse, depicted in Figure 2, underwent measurements using a pressure and flow meter (DT-8920, CEM) to determine air velocities. The baghouse's total height was 2.5 m, and the cross-section of the chamber measured 0.75×0.75 m. Airflow measurements were taken inside the inlet duct at points V1 and V2 to assess filtration velocity, and inside the exhausting air duct at point V3 to determine outlet velocity. Point V2, relevant to filtration velocity, was positioned 0.40 m away from the baghouse wall, with a distance of 1.10 m from V2 to V1. The length of the exhausting air duct from the baghouse wall to the V3 position was 0.65 m. Pressure drop values were measured between the housing (P1) and top (P2) chambers using the pressure and flow meter, which had an accuracy of ±2.5% and ±0.3% for velocity and pressure, respectively. Five different filtration velocities were achieved by adjusting the blower's frequencies from 10 to 50 Hz, with a frequency step interval of 10 Hz.

The bag filter employed in the study was of a cylindrical type and crafted from nonwoven material. The specific nonwoven fabric used, designated as PE/PE 404 glaze CS17 and provided by the manufacturer (BWF Envirotec), is detailed in Table 1. Throughout all testing cases, this bag filter remained consistent. The experiments were conducted repetitively, with each test repeated five times at every outlet air velocity.

Table 1 Technical data of nonwoven fabric

Description	Value
Composition	
-Web	Polyester
-Scrim	Polyester
Area Weight (g/m2)	400
Thickness (mm)	1.3
Density (g/cm3)	0.31
Air Permeability (mm/s @ 200 Pa)	300
Tensile Strength	
- Length (N)	1,500
- Cross (N)	1,500
Temperature Resistance	
- Cont. (°C)	< 150
- Peak (°C)	< 150

Nonwoven textiles are produced through a process that begins with the formation of a web using constituent fibers or filaments, followed by the mechanical, thermal, or chemical bonding of these elements. The orientation of these fibers or filaments within the nonwoven textiles can be either random or preferential. Figure 3 visually presents the oriented filaments of the PE/PE 404 glaze CS17 through scanning electron microscopy (SEM). It's worth noting that the photograph was taken on a scale of 500 micrometers, providing a detailed perspective on the oriented filaments.

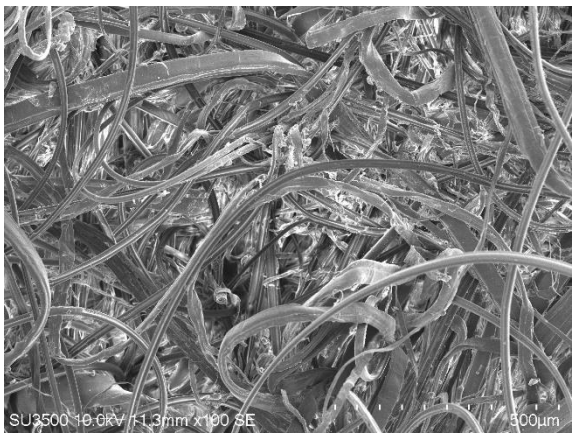

Fig.3 The PE/PE 404 glaze CS17 filament arrangement.

4.2 Baghouse Filter Modeling

The computational domain of the baghouse filter is shown in Fig. 4, where we simplified the shape by leaving out unnecessary parts like legs, blower, and sections of the outlet duct. We used tetrahedral cells for meshing this domain. A grid independence study was carried out to assess the quality of the cell structure, with the pressure difference between both chambers of the bag-housed filter as the study criterion. The results of the grid independence study are illustrated in Fig. 5. A total of 14,186,956 cells met the criteria for grid independence, representing different pressures of 65 Pa, which differed from the total of 15,000,000 cells at 14.17 Pa. The 14,186,956 cells gave pressures different from the 12,700,000 cells at 7.76 Pa, but the results matched well with experimental data. Notably, the cells on the bag filter were refined to achieve a y+ value of 1.0. The airflow velocity, ranging from 0.5 to 3.0 m/s, was assigned to the outlet duct at the V3 position. Initial pressures inside and outside the baghouse filter model were set at atmospheric pressure (101,325 Pa). The bag filter was treated as a porous medium, with porous properties obtained from experimental data.

The finite-volume-based open-source Computational Fluid Dynamics (CFD) software, OpenFOAM, was employed to discretize and solve

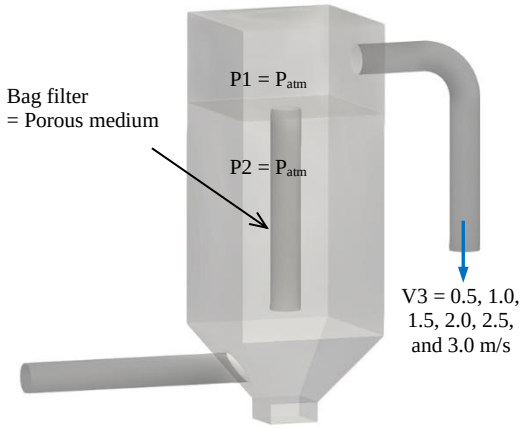

Fig. 4 The CFD model of the baghouse

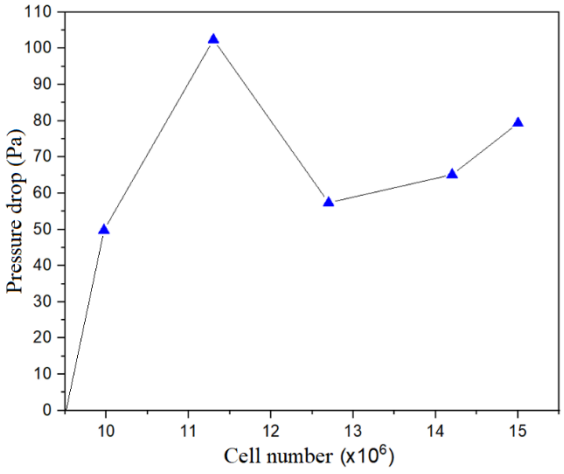

Fig. 5 Pressure drop vs. cell number graph

the governing equations [16-18]. The convective term in the momentum equation was discretized using the linear upwind scheme, while the diffusive term was discretized using the central scheme. The pressure-velocity coupling problem was addressed using the SIMPLE algorithm. To ensure the convergence of the CFD results, residual control was implemented for each parameter. The simulations concluded when the initial residual fell below the specified control values, set at 10^{-3} and 10^{-5} for pressure and velocity, respectively, as defined in this research. All simulations were executed on Ubuntu-based Linux using a CPU Intel Core i7 with 2.10 GHz and 16.00 GB RAM.

5. RESULTS AND DISCUSSION

This section presents experiment and CFD outcomes, comparing them for equation accuracy confirmation. Analyzing differences, acknowledging limitations, and discussing implications highlight the study's significance, contributing to a broader understanding of the subject.

5.1 Bag Filter Properties

The blower systematically increased the outlet velocity from 0.5 to 3.0 m/s in 0.5 m/s increments for measuring both inlet and outlet velocities and pressures. The pressure drops, a direct consequence of the flow rate through the bag filter, exhibited an increase in tandem with the flow rate. As illustrated in Fig. 6, the pressure drop was observed to rise with filtration velocity. By modeling the pressure drop across the bag filter, as shown in Fig. 3, using Eq. (8), two coefficients multiplying with the velocity were obtained. Subsequently, the linear resistance coefficient (D) and quadratic resistance coefficient (F) were determined using Eq. (8), with coefficients (D and F) set at 3.50×107 and 0, respectively. This configuration aligned the pressure drop of the bag filter with Darcy's law, as supported by the work of Cao et al. [19].

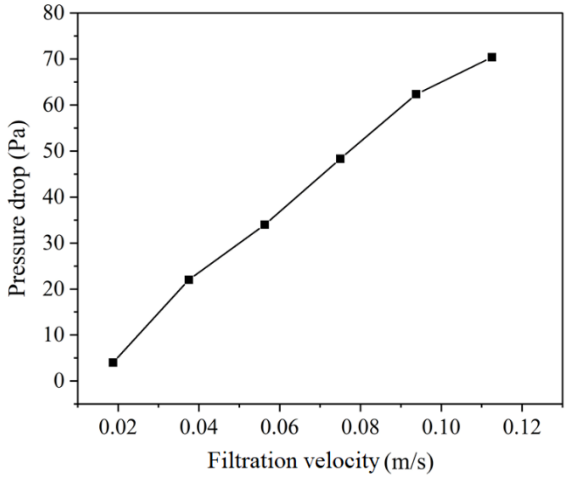

Fig. 6 Pressure drop vs. filtration velocity graph

5.2 Validation

In Figure 7(a), the pressure contour inside the baghouse is depicted with an outlet velocity assignment of 3.0 m/s. Notably, the pressure was observed to be low in the outlet duct, measuring -70.41 Pa. Although the stream tracer indicated turbulent flow, the pressure inside the top and housing chambers exhibited explicit differences yet remained almost uniform. Specifically, the pressure inside the top chamber of the baghouse decreased to -67.91 Pa, while the housing chamber, where the air was drawn

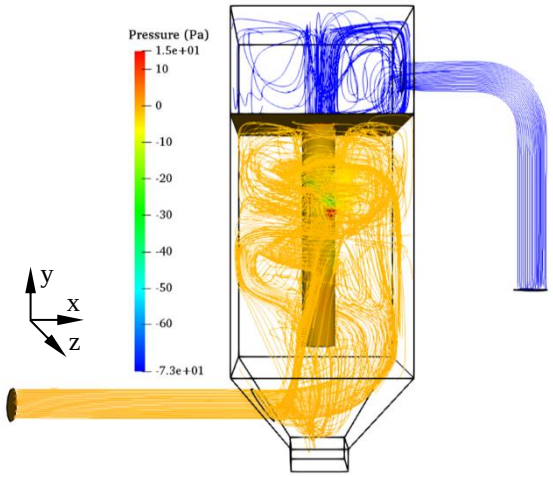

(a)

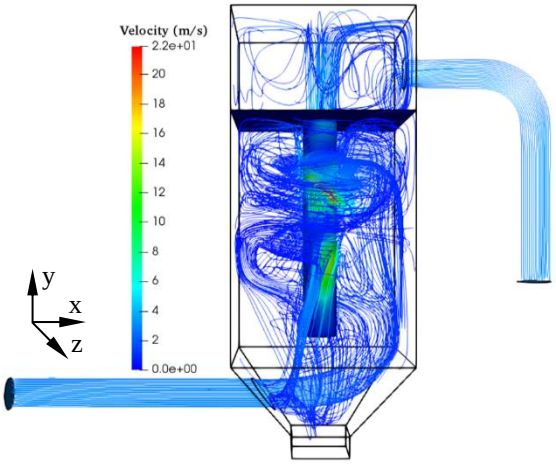

(b)

Fig. 7 Contour and stream tracer of (a) pressure and (b) velocity inside the baghouse model

in, maintained a pressure of -3 Pa. Consequently, the pressure drop attributed to the outlet air velocity of 3.0 m/s amounted to 70.91 Pa.

In Figure 7(b), the velocity tracer and contour inside the baghouse are displayed at the same outlet velocity as in Figure 7(a). The color contour represents the values of air velocity, with the velocity at the outlet matching the assigned value, while the inlet air velocity was 3.05 m/s. The maximum airflow velocity was observed at the outlet, precisely at 3.0 m/s. The filtration velocity, visible on the surface of the bag filter in this assigned outlet air velocity, was calculated to be 0.11 m/s. The stream tracer inside the baghouse indicated a turbulent flow, with the observation that the flow direction did not fully impinge on the outer surface of the bag filter, influencing the position of the inlet duct.

The comparison between CFD and the experiment involves using pressure drop values. The percentage error of the CFD can be calculated using the following equation:

$$Percentage\ error = \left|\frac{CFD - Exp.}{Exp.}\right| \times 100\% \quad (9)$$

where CFD and $Exp.$ denote CFD and experiment results, respectively.

Figure 8 presents a comparison between the pressure drop at each filtration velocity obtained from the simulation and experimental data. The pressure drop values from the experiment and CFD were juxtaposed for validation, and the results of this comparison are outlined in Table 2. It was noted that the error increased at higher filtration velocities, suggesting that a y+ value equal to 1 might be inappropriate for high outlet air velocities. Despite this, the CFD results demonstrated good agreement with the experimental data, with an average error of less than 6.46%. The ability of high velocity to effectively draw dust into the baghouse depends on the porous properties of bag filters. Therefore, the selection of an appropriate bag filter can be informed by an investigation into airflow velocity within the baghouse model. In subsequent work, CFD will be instrumental in designing the bag filter.

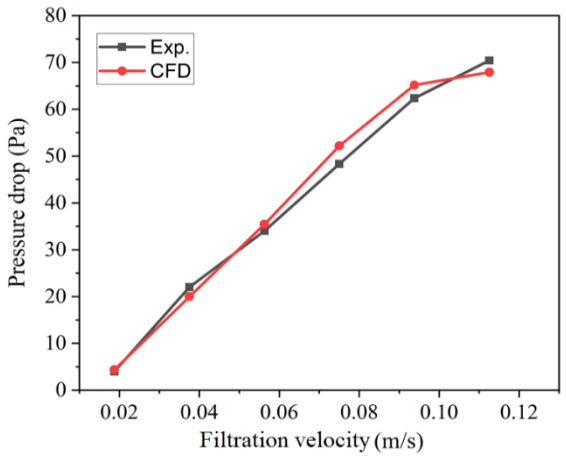

Fig. 8 Pressure drop vs. filtration velocity graphs of CFD and experiment

Table 2 Comparison results

Outlet air velocity (m/s)	Filtration velocity (m/s)	Pressure drop (Pa)		Error (%)
		Experiment	CFD	
0.5	0.018	4.00	4.38	9.50
1.0	0.037	22.00	20.00	9.09
1.5	0.056	34.00	35.42	4.17
2.0	0.075	48.31	52.17	7.99
2.5	0.938	62.35	65.14	4.47
3.0	0.112	70.41	67.91	3.55

The equipment's filtration effectiveness hinges on the mass flow profile within bags and the filtration cycle duration. A more uniform gas mass flow distribution, influenced by filter fluid dynamics, enhances filtration cycles, extending bag lifespan and reducing maintenance frequency. Utilizing CFD simulations offers insights challenging to obtain experimentally. For instance, Fig. 9 visually illustrates concentrated mass flow in specific feed region areas, with the majority passing through bags highlighted in red. The baghouse's maximum mass flux, with a single bag filter, reached 25.70 Kg/(m^{2}s).

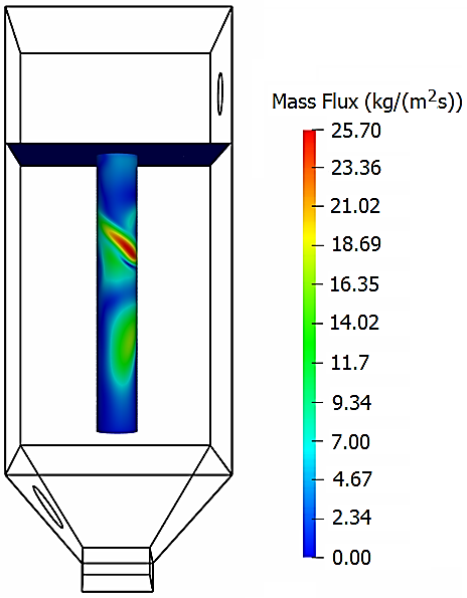

Fig. 9 Mass flux on the bag filter

6. CONCLUSIONS

This study utilized the OpenFOAM software to model a baghouse, with the primary objective of investigating airflow within the system to guide the selection of appropriate porous properties for the bag filter. The key findings and conclusions of this work are summarized as follows:

1) The baghouse, equipped with a bag filter, was physically fabricated to determine the properties of

the porous medium, specifically the linear and quadratic resistance coefficients. Notably, the technical data of the nonwoven fabric did not include information about these porous medium properties.

2) The pressure drop across the bag filter exhibited an increase corresponding to the rise in filtration velocity, aligning with Darcy's law.

3) The k-ε turbulence model proved effective in predicting the pressure drop and filtration velocity of the baghouse model. The outlet airflow velocity was varied from 0.5 to 3.0 m/s, and the model demonstrated accurate predictions, with an average error of less than 2.25%.

4) The positioning of the air inlet duct played a crucial role in controlling the stream tracer of air. Optimal airflow impinging throughout the bag filter surface was identified as a key factor for achieving high bag filter efficiency.

5) The equipment's filtration effectiveness depends on mass flow within bags and filtration cycle duration. A uniform gas mass flow distribution, influenced by filter fluid dynamics, improves cycles and extends bag lifespan, reducing maintenance frequency. Computational Fluid Dynamics (CFD) simulations excel in providing hard-to-obtain experimental insights.

6) The developed CFD model of the baghouse filter provides a valuable tool for investigating stream tracer patterns and airflow velocities, facilitating the informed selection of nonwoven fabric properties for the bag filter. This approach contributes to the optimization and design of baghouses in future applications.

7. ACKNOWLEDGMENTS

This research was made possible through the generous financial support from the Thailand Research Fund (TRF) and Dust Control Co., Ltd., granted under the TRF Research Grant No. MSD62I0010. We extend our gratitude to these organizations for their crucial contributions to our study. Their funding has played a pivotal role in enabling and advancing our research endeavors. This acknowledgment underscores the significance of their support, emphasizing the collaborative nature of this project and the valuable partnership with Dust Control Co., Ltd. and the TRF.

8. REFERENCES

[1] Litchwark J.O., Winchester J., and Nijdam J. J., Design of pulse-jet systems for milk powder baghouses. Powder Technol, Vol. 284, 2015, pp. 379-386.

[2] Rogozinski T., Pilot-scale study on the influence of wood dust type on pressure drop during filtration in a pluse-jet baghouse. Process Safety and Environmental Protection, Vol. 119, 2018, pp. 58-64.

[3] Zheng C. H., and Kanaoka C., Recent advances in dust collection technology and ISO standardization in bag filtration, Journal of Zhejiang University-SCIENCE A (Applied Physics & Engineering), Vol. 19, 2018, pp. 21-33.

[4] Yeo S. Y., Kim O. S., Lim D. Y., and Byun S. W., Effect of processing condition on the filtration performances of nonwovens for bag filter media, Journal of Materials Science, Vol. 40, 2005, pp. 5393-5398.

[5] Kim J. U., Hwang J., Choi H. J., and Lee M. H., Effective filtration area of a pleated filter bag in a pulse-jet baghouse. Powder Technology, Vol. 311, 2017, pp. 522-527.

[6] Kim J. S., and Lee M. H., Measurement of effective filtration area of pleated bag filter for pulse-jet cleaning. Powder Technology, Vol. 343, 2019, pp. 662-670.

[7] Joe Y. H., Shim J., and Park H. S., Evaluation of can velocity effect on a bag filter. Powder Technology, Vol. 321, 2017, pp. 454-457.

[8] Pereira T. W. C., Marques F. B., Pereira F. A. R., Ribeiro D. C., and Rocha S. M. S., The influence of the fabric filter layout of in a flow mass filtrate. Journal of Cleaner Production, Vol. 111, 2016, pp. 117-124.

[9] Park S., Joe Y. H., Shim J., Park H., and Shin W. G., Non-uniform filtration velocity of process gas passing through a long bag. Journal of Hazardous Materials, Vol. 365, 2019, pp. 440-447.

[10] Lin L., Liu T., Yuan N., Xu Z., and Chen H., Study on the influence of venture on the cleaning performance of elliptical filter cartridge. Powder Technology, Vol. 377, 2021, pp. 139-148.

[11] Loksupapaiboon K., and Suvanjumrat C., Effects of flow and heat transfer around a hand-shaped former. Engineering Applications of Computational Fluid Mechanics, Vol. 16, Issue 1, 2022, pp. 1619-1640.

[12] Loksupapaiboon K., and Suvanjumrat C., Forced convective heat transfer and fluid flow past a rotating hand-shaped former for improving rubber glove curing. Case Studies in Thermal Engineering, Vol. 47, 2023, pp. 103050.

[13] Suvanjumrat C., Implementation and validation of OpenFOAM for thermal convection of airflow. Engineering Journal, Vol. 21, Issue 5, 2017, pp.

225-241.

[14] Simmons C. T., Henry Darcy (1803–1858): Immortalised by his scientific legacy. Hydrogeology Journal, Vol. 16, 2008, pp. 1023-1038.

[15] Ehlers W., Darcy, Forchheimer, Brinkman and Richards: classical hydromechanical equations and their significance in the light of the TPM, Archive of Applied Mechanics, Vol. 92, 2022, pp. 619-639.

[16] Chaichanasiri, E. and Suvanjumrat, C., Simulation of three dimensional liquid-sloshing models using C++ open source code CFD software. Kasetsart Journal (Natural Science), Vol. 46, Issue 6, 2012, pp. 978–995.

[17] Kamma, P. and Suvanjumrat, C., A novel diffusion flux modeling for laminar premixed flame simulation with OpenFOAM. Results in Engineering, Vol. 20, 2023, pp. 101462.

[18] Suvanjumrat, C. and Loksupapaiboon, K., Improvement of thermal distribution in the rubber-glove former conveyor oven by openFOAM. Engineering Journal, Vol. 24, Issue 2, 2020, pp. 109-120.

[19] Cao B., Qian F., Ye M., Guo Y., Wang S., Lu J., and Han Y., Pressure drop model for fibrous media in depth filtration: Coupling simulation of microstructure and CFD porous media during dust loading. Building and Environment, Vol. 202, 2021, pp. 108015.